https://doi.org/10.5194/hess-2021-244
Preprint. Discussion started: 28 May 2021

Hydrology and Earth System Sciences
Discussions
Open Access
EGU

Can we use precipitation isotope outputs of Isotopic General Circulation Models to improve hydrological modeling in large mountainous catchments on the Tibetan Plateau?

Yi Nan[1], Zhihua He[2], Fuqiang Tian[1], Zhongwang Wei[3], Lide Tian[4]

[1] Department of Hydraulic Engineering, State Key Laboratory of Hydroscience and Engineering, Tsinghua University, Beijing 100084, China

[2] Center for Hydrology, University of Saskatchewan, Saskatchewan, Canada

[3] Guangdong Province Key Laboratory for Climate Change and Natural Disaster Studies, School of Atmospheric Sciences, Sun Yat-sen University, Guangzhou, Guangdong, China

[4] Institute of International Rivers and Eco-security, Yunnan University, Kunming, China

***Corresponding to*:** Fuqiang Tian

Address: Room 330 New Hydraulic Building, Tsinghua University, Beijing 100084, China

Email: tianfq@mail.tsinghua.edu.cn

https://doi.org/10.5194/hess-2021-244
Preprint. Discussion started: 28 May 2021

Hydrology and Earth System Sciences
Discussions
Open Access
EGU

15 **Abstract**

16 Issues related to large uncertainty and parameter equifinality have posed big challenges
17 for hydrological modeling in cold regions where runoff generation processes are particularly
18 complex. Tracer-aided hydrological models coupling modules to simulate the transportation
19 and fractionation of water stable isotope are increasingly used to constrain parameter
20 uncertainty and refine the parameterizations of specific hydrological processes in cold regions.
21 However, commonly unavailability of site sampling of spatially-distributed precipitation
22 isotope hampers the practical applications of tracer-aided models in large scale catchments.
23 This study, taken the precipitation isotope data (isoGSM) derived from the Isotopic General
24 Circulation Models (iGCM) as an example, explored its utility in driving a tracer-aided
25 hydrological model in the Yarlung Tsangpo River basin (YTR, around 2×10^5 km^2) on the
26 Tibetan Plateau (TP). The isoGSM product was first corrected based on the biases between
27 gridded precipitation isotope estimates and limited site sampling measurements. Model
28 simulations driven by the corrected isoGSM data were then compared with those forced by
29 spatially interpolated precipitation isotope from site sampling measurements. Our results
30 indicated that: (1) spatial precipitation isotope derived from the isoGSM data helped to reduce
31 modeling uncertainty and improve parameter identifiability in a large mountainous catchment
32 on the TP, in comparison to a calibration method using discharge and snow cover area fraction
33 without any information of water isotope; (2) model parameters estimated by the corrected
34 isoGSM data presented higher transferability to nested sub-basins and produced higher model
35 performance in the validation period than that estimated by the interpolated precipitation
36 isotope data from site sampling measurements; (3) model calibration procedure forced by the
37 corrected isoGSM data successfully rejected parameter sets that overestimated glacier melt
38 contribution and gave more reliable contributions of runoff components, indicating the
39 corrected isoGSM data served as a better choice to provide informative spatial precipitation
40 isotope than the interpolated data from site sampling measurements at macro scale. This work
41 suggested plausible utility of combining isoGSM data with measurements from a sparse
42 sampling network in improving hydrological modeling in large mountainous catchments.

43 **Key word**

44 Tracer-aided hydrological modeling; Large basins on the Tibetan Plateau; Isotopic General
45 Circulation Models (iGCM) product; Combining isoGSM isotope data with measurements at
46 sparse sampling sites.
47

https://doi.org/10.5194/hess-2021-244
Preprint. Discussion started: 28 May 2021

Hydrology and Earth System Sciences
Discussions
Open Access
EGU

1. Introduction

Large uncertainty and strong equifinality of parameter calibration are the widely faced issues in hydrological modelling (Gupta et al., 2008), especially in cold regions where hydrological complexity is highly enhanced by the competitions of multiple water inputs and the strong spatio-temporal variabilities of runoff generation processes (Zongxing et al., 2019). Tracer-aided hydrological models integrating a water or environmental tracer (e.g., stable oxygen isotope, $\delta^{18}O$) module into the runoff generation architecture have been proved as highly valuable in improving parameter calibration and diagnosing model uncertainty (Son and Sivapalan, 2007; Birkel et al., 2011; Capell et al., 2012; He et al., 2019). However, practical applications of tracer-aided hydrological modeling are mainly limited in only small to meso scales. The largest basin area where previous tracer-aided modelling works have been successfully implemented is around 10^3 km^2 (e.g., Delavau et al., 2017; Campell et al., 2012; Stadnyk et al., 2013). Reasons fall in either the lumped conceptual model structures (Birkel and Soulsby, 2015), which are particularly not suitable for capturing the strong spatial variability of hydrological behaviors in large scale basins, or the low availability of tracer data in large basins due to difficulties in the long-term, continuous and high-frequency field sampling works (e.g., Ala-aho et al., 2017; He et al., 2019).

The Tibetan Plateau (TP) is the source region of several large rivers (e.g., Brahmaputra, Ganges), which sustain the ecosystems and provide a great proportion of water source for downstream livelihoods and agricultural irrigation (Zhang et al., 2013; Schaner et al., 2012). Decision making of water resource management over TP and its downstream area relies heavily on river runoff in the large basins. Meanwhile, melting water from snow and ice contributes a large proportion to river runoff in the large basins on TP due to the cold climate and glacier coverage in head watersheds (Zongxing et al., 2019). Runoff in this region is thus highly vulnerable to climate warming. Robust quantification of the contribution of meltwater to river runoff is critical in understanding water resources dynamics on TP (Immerzeel et al., 2013). Although great efforts have been taken to quantify the contributions of runoff components (e.g., Immerzeel et al., 2010; Lutz et al., 2014) and their future trends under climate changes on TP (e.g., Su et al., 2016; Masood et al., 2015), results reported in the wide range of studies show substantial differences (Xu et al., 2019; Tian et al., 2020), which indicate big challenges on quantifying contributions of runoff components and predicting their future trend in the large basins on TP. The difficulty of this task is mainly related to the large uncertainty of hydrological modelling and parameter calibration in the TP, because of the complex hydrological processes (He et al., 2018) and the commonly inaccurate estimation of precipitation (Xu et al., 2017; He et al. 2017). The strong inter-competitions of runoff processes induced by meltwater and

https://doi.org/10.5194/hess-2021-244
Preprint. Discussion started: 28 May 2021


Hydrology and Earth System Sciences
Discussions
Open Access
EGU

rainwater were inadequately constrained in hydrological models by the commonly used hydrological observation of streamflow (Duethmann et al., 2015), and even additional data of snow/ice coverage (He et al. 2019) which further enhanced the equifinality issue of parameter identification in large basins on TP. Reducing the modelling uncertainty originated from parameter calibration is essential for proper understanding of runoff regimes and robust prediction of future hydrological change.

Tracer-aided hydrological models that additionally involved water stable isotope data for parameter calibration have been proved as highly capable on constraining the inter-competitions of runoff processes induced by meltwater and rainwater in high mountains (He et al. 2019; Nan et al. 2021), which, however, have not been tested in large basins yet due to the unavailability of precipitation isotope data. Global gridded isotope product potentially serves as an alternative forcing of precipitation isotope data for tracer-aided hydrological models in large basins where high-frequency sampling work in a large region is not feasible. One of these options comes to outputs of the isotopic General or Regional Circulation Models (iGCM and iRCM, Noone and Sturm, 2010; Xi, 2014; Sturm et al., 2005, 2007), which has been proved to have high performance on simulating the seasonal and spatial variations of isotopic signature of precipitation on regional and global scales (Wang et al., 2017; Yao et al., 2013). However, very few works have been conducted to test the behavior of such products on forcing hydrological models. To the best of our knowledge, the only one work was conducted by Delavau et al. (2017), who examined the performance of an iRCM product REMOiso on forcing tracer-aided model in a regional catchment of around 10^3 km^2 in Canada. Their results indicated that hydrological simulations driven by the iRCM product reproduced the variations of isotopic signature ($\delta^{18}O$) of river water comparably to the simulations driven by $\delta^{18}O$ measurements from sampling sites and improved the representations of internal hydrological processes in the model. Those attempts provide sound confidences for exploring the utility of global and regional gridded isotope data products in aiding hydrological modeling in large basins on TP.

Motivated by the mentioned backgrounds, we adopted a tracer-aided hydrological model developed by Nan et al. (2021) to simulate runoff processes and the contributions of runoff components to streamflow in a large basin extending around 2×10^5 km^2 on the TP. The isotope module was driven by two kinds of precipitation isotope data including site measurements from water samples and outputs of iGCM. Scientific questions addressed in this study are two-fold: (1) what are the benefits of involving water isotope data for hydrological modeling in larger catchments? (2) how does the gridded precipitation isotope data of iGCM products perform on forcing tracer-aided hydrological model in large basins?

https://doi.org/10.5194/hess-2021-244
Preprint. Discussion started: 28 May 2021


Hydrology and Earth System Sciences
Discussions
Open Access
EGU

2. Materials and methodology

2.1 Study area

The Yarlung Tsangpo River (YTR) located in the southern TP on the north of Himalaya Mountain (Fig. 1) is one of the longest rivers (longer than 2000 km) originating from TP. The YTR basin is located in the range of 27-32°N and 82-97°E, with an elevation range of 2900-6900 m a. s. l. The mean annual precipitation in YTR basin is around 470 mm, which is dominated by South Asian Monsoon in the Indian Ocean hydrosphere-atmosphere system, resulting in obvious wet season from June to September (Dong et al., 2016). Contributing area to the Nuxia hydrological station extends approximately 2×10^5 km^2, around 2% of which is covered by glacier. Plenty of previous works have shown the great contribution of snow and glacier melting to the runoff in YTR (e.g., Chen et al., 2017; Tian et al., 2020).

The Karuxung River (KR) catchment is located in the upper region of YTR basin, on the northern slope of the Himalayan Mountains, which is used for model evaluation in sub-basin because of its high glacierized area proportion (around 20%). The KR originates from the Lejin Jangsan Peak of the Karola Mountain at 7206 m above sea level (a.s.l.), and flows into the Yamdrok Lake at 4550m a.s.l. (Zhang et al., 2006). The KR catchment covers an area of 286 km^2. Runoff in KR catchment is strongly influenced by the headwater glaciers which cover an area of around 58 km^2.

[Figure 1]

2.2 Hydro-meteorological data and site water sampling for isotope analysis

Digital elevation model (DEM) data in the YTR catchment with a spatial resolution of 30-m was extracted from the Geospatial Data Cloud (http://www.gscloud.cn). The 3-hour 0.1°×0.1° China Meteorological Forcing Dataset (CMFD) which combined multiple datasets (e.g., GLDAS and TRMM) with the national meteorological station data (Yang et al., 2010) provided meteorological inputs including precipitation, temperature and potential evapotranspiration. Glacier coverages were extracted from the Second Glacier Inventory Dataset of China (Liu, 2012). The Tibetan Plateau Snow Cover Extent product (TPSCE, 5km×5km, Chen et al., 2018) were used to denote the fluctuations of daily snow cover area (SCA) in the basins. The 8-day Leaf Area Index (LAI) and the monthly normalized difference vegetation index (NDVI) data were downloaded from MODIS products of MOD15A2H (500m×500m, Myneni et al., 2015) and MOD13A3 (1km×1km, Didan, 2015), respectively. Soil parameters were estimated based on the soil properties extracted from the 1km × 1km Harmonized World Soil Database (HWSD, http://www.fao.org/geonetwork).

Daily streamflow during 2000-2010 for hydrological calibration were observed at the Nuxia, Yangcun and Nugesha hydrological stations. Grab samples of precipitation and stream water were collected in 2005 at four stations along the main stream of YTR, i.e., Lazi (4889 m

https://doi.org/10.5194/hess-2021-244
Preprint. Discussion started: 28 May 2021


Hydrology and Earth System Sciences
Discussions
Open Access
EGU

a.s.l.), Nugesha (4715 m a.s.l.), Yangcun (4541 m a.s.l.) and Nuxia (3691 m a.s.l.), from the upstream to the downstream (Fig. 1). Precipitation water were sampled as immediately as possible after the precipitation events, and stream water samples were collected weekly every Monday from the river. Considering the west-east flowing direction of the river (Fig. 1b) and the effect of altitude, the measured isotopic composition of precipitation from site sampling was interpolated by longitude and altitude (similar with Zhao et al. 2012, Liu et al. 2014) using Eq. 1 to provide spatial precipitation isotope for model input, in which the coefficients x, y and z were estimated by least squares fitting the average precipitation $\delta^{18}O$ and corresponding altitude/longitude at the four measuring stations. Isotopic composition of glacier meltwater was assumed to be constant during the entire study period, and lower than the amount weighted average isotopic composition of precipitation.

$$\overline{\delta^{18}O_{precipitation}}(‰) = x * ALT(m) + y * LON(°E) + z \quad (1)$$

Daily temperature and precipitation in the KR catchment during 2006-2012 were collected at the Langkazi meteorological Station. Altitudinal distributions of temperature and precipitation across the catchment were estimated by the lapse rates reported in Zhang et al. (2015). Daily streamflow during 2006-2012 for hydrological calibration and evaluation were measured at the Wengguo hydrological station. Grab samples of precipitation and stream water at the Wengguo Station in 2006-2007 and 2010-2012 were collected for isotope analysis. Isotopic composition of precipitation over elevation bands was calculated from the sampling site of Wengguo Station using an altitudinal lapse of -0.34‰/100m reported in Liu et al. (2007). Isotopic composition of glacier meltwater in this catchment was assumed to be -18.9‰, constantly throughout the entire study period, adopting from the value reported in Gao et al. 2009). Details of water samples in YTR and KR catchments are summarized in Table 1.

[Table 1]

2.3 Isotopic General Circulation Model isoGSM and bias correction

Precipitation $\delta^{18}O$ of the Scripps global spectral model with water isotopes-incorporated (isoGSM) developed by Yoshimura et al. (2008) was extracted to drive the tracer-aided model. IsoGSM was developed from the Scripps Experimental Climate Prediction Center's GSM, which was based on the medium range forecast model for making operational analysis and predictions (Kanamitsu et al., 2002). According to a previous comparison of ten iGCMs in Wang et al. (2017), the isoGSM product showed the best performance on simulating global spatial pattern of precipitation $\delta^{18}O$. The spatial and temporal resolutions of isoGSM dataset are 1.875°×1.875° and 6 hours, respectively.

The precipitation $\delta^{18}O$ estimated by isoGSM was corrected by site sampling measurements in Eqs. 2-4 before used for hydrological model input. Biases between the amount weighted averages of isoGSM isotope and sampling measurement at the four sampling sites in YTR basin

https://doi.org/10.5194/hess-2021-244
Preprint. Discussion started: 28 May 2021


Hydrology and Earth System Sciences
Discussions

were calculated in Eq. 2 first. Spatial distribution of bias between isoGSM isotope and sampling measurement was then assumed as linearly related to altitude in Eq. 3, in which the coefficients of a and b were estimated by least squares fitting the site biases calculated in Eq. 2 and corresponding site altitudes. Daily isoGSM isotope data in hydrological model units over the study catchment were finally corrected in Eq. 4 using the unit altitudes.

$$bias_i = \overline{\delta^{18}O_{i,m}} - \overline{\delta^{18}O_{i,G}} \quad i = 1,2,3,4 \tag{2}$$

$$bias\_r = a * ALT + b \tag{3}$$

$$\begin{cases} bias\_r_i = \delta^{18}O_{i,j,G} + a * ALT_i + b \\ \delta^{18}O_{i,j,Corr} = \delta^{18}O_{i,j,G} + bias\_r \end{cases} \tag{4}$$

where, $\overline{\delta^{18}O_{i,m}}$ is the amount weighted average of measured precipitation isotope over the sampling period in site i (i=1-4), and $\overline{\delta^{18}O_{i,G}}$ is the amount weighted average of isoGSM precipitation isotope over the study period in pixel that contains the sampling site i. *ALT* is altitude of the sampling site or hydrological model unit. Parameters a and b are the linear regression coefficients. $\delta^{18}O_{i,j,Corr}$ and $\delta^{18}O_{i,j,G}$ are the corrected and original isoGSM precipitation isotope at hydrological model unit i (i=1-63) on the j^{th} day, respectively. Performance of the correction method of isoGSM data was evaluated by sampling measurement of precipitation isotope at the Wengguo station in the KR sub-basin, which was not involved in the estimation of coefficients a and b in Eq. 3. Spatial precipitation isotope of the isoGSM data in the KR sub-basin for hydrological modeling was estimated using the same altitudinal lapse that was used to interpolate the sampling data in Section 2.2, because the KR catchment only encompasses one pixel of the isoGSM data.

2.4 Tracer-aided hydrological model

A distributed tracer-aided hydrological model THREW-t (Tian et al., 2006; Nan et al., 2021) was adopted in this study for streamflow and isotope simulations. This model uses the Representative Elementary Watershed (REW) method for the spatial discretization of catchment, in which the study catchment is first divided into REWs based on the catchment DEM. Each REW is further divided into hydrological sub-zones using land covers and soil properties within the REW. In total, 63 and 41 REWs were extracted in YTR and KR, respectively. Areal averages of the gridded estimates of CMFD meteorological variables and precipitation $\delta^{18}O$ were used in each of the REWs to drive the hydrological model. For application in cold and high regions, a module representing the glacier melting and snowpack evolution was incorporated into the original model in Tian et al. (2006), which has been proved as successful in previous modelling works (e.g., He et al., 2015; Xu et al., 2019; Tian et al., 2020). The tracer module was developed by Nan et al. (2021) which performed quite well on reproducing the isotopic signature of stream water in the KR catchment. The isotope mixing

https://doi.org/10.5194/hess-2021-244
Preprint. Discussion started: 28 May 2021


Hydrology and Earth System Sciences
Discussions
Open Access
EGU

and fractionation processes were simulated based on the completely mixing assumption and the Rayleigh fractionation method (Hindshaw et al., 2011; Wolfe et al., 2007). More details of model description and set up are given in Tian et al. (2006) and Nan et al. (2021).

The physical basis and value ranges of the calibrated parameters in the THREW-t model are described in Table 2. In both modeling catchments of YTR and KR, the parameter values were optimized using three calibration variants: (1) a dual-objective calibration using observed discharge and MODIS snow covered area fraction (SCA), (2) a triple-objective calibration using observed discharge, MODIS SCA and $\delta^{18}O$ measurements of stream water forced by linearly interpolated measurements of site sampling precipitation isotope, and (3) a triple-objective calibration using observed discharge, MODIS SCA and $\delta^{18}O$ measurements of stream water but forced by the isoGSM precipitation isotope data. Metrics used to evaluate the simulations of discharge, SCA and isotope are list in Eqs. 5-7.

$$NSE_{dis} = 1 - \frac{\sum_{i=1}^{n}(Q_{o,i}-Q_{s,i})^2}{\sum_{i=1}^{n}(Q_{o,i}-\overline{Q_o})^2} \quad (5)$$

$$RMSE_{SCA} = \sqrt{\frac{\sum_{i=1}^{n}(SCA_{o,i}-SCA_{s,i})^2}{n}} \quad (6)$$

$$MAE_{iso} = \frac{\sum_{i=1}^{n}\left|\delta^{18}O_{o,i}-\delta^{18}O_{s,i}\right|}{n} \quad (7)$$

where, n is the total number of observations. Subscripts of o and s refer to observed and simulated variables, respectively. $\overline{Q_o}$ is the average value of observed streamflow during the assessing period.

[Table 2]

An automatic procedure based on the pySOT optimization algorithm developed by Eriksson et al. (2015) was implemented for all the three calibration variants to identify the behavioral parameters. The pySOT used surrogate model to guide the search for improved solutions, with the advantage of needing few function evaluations to find a good solution. An event-driven framework POAP were used for building and combining asynchronous optimization strategies. The optimization was stopped if a maximum number of allowed function evaluations was reached, which was set as 3000 in this study. For both modeling catchments, the pySOT algorithm was repeated 150 times for each calibration variant. Although the measurement unit of NSE_{dis} is different from $RMSE_{SCA}$ and MAE_{iso}, their values are in the same order of magnitude when the model performances were acceptable (Ala-aho et al., 2017; Nan et al., 2021). Consequently, they were combined with equal weights to reflect the simultaneous performance on multiple objectives. For the dual- and triple-objective calibration variants, NSE_{dis} - $RMSE_{SCA}$, NSE_{dis} - $RMSE_{SCA}$ - MAE_{iso} were chosen as combined optimization objectives, respectively. Among the 150 final parameter sets produced by the pySOT runs, the behavioral parameter sets were selected by NSE_{dis} thresholds, i.e., only the parameter sets producing NSE_{dis} higher than an assumed threshold were regarded as behavioral parameter sets.

https://doi.org/10.5194/hess-2021-244
Preprint. Discussion started: 28 May 2021


Hydrology and Earth System Sciences
Discussions
Open Access
EGU

For the YTR catchment, the NSE_{dis} threshold was chosen as 0.85. For KR catchment, the threshold was chosen as 0.75 and 0.70 for dual- and triple-objective calibration variants, respectively.

Considering the data availability, the calibration and validation periods for KR catchment were set as 2006-2010 and 2011-2012, respectively. For YTR basin, discharge measured at the outlet station Nuxia, the MODIS SCA fraction over the basin area upper the Nuxia station, and the stream water $\delta^{18}O$ measured at the Nuxia station were used for calibration. Calibration and validation periods of 2001-2005 and 2006-2010 were selected to test the model performance for simulations of discharge and SCA at the Nuxia station. In addition, discharge measured at the internal hydrological stations of Yangcun and Nugesha during 2001-2010 were used to validate the spatial consistency of the calibrated model parameters. Model performance on simulating stream water isotope at the Nuxia station in a validation period was not assessed as stream water isotope measurements were available only during 2005. However, stream water $\delta^{18}O$ measured during 2005 at the internal hydrological stations of Yangcun, Nugesha and Lazi were adopted to validate the model performance on simulating spatial stream water $\delta^{18}O$ within YTR basin.

3. Results

3.1 Comparison between isoGSM and measured precipitation $\delta^{18}O$

Figs. 2a and 3a show the comparison between isoGSM and measured precipitation $\delta^{18}O$ at four sampling sites in the YTR basin. The isoGSM data presented similar fluctuations of seasonal precipitation $\delta^{18}O$ to the sampling measurements (Fig. 3a). In particular, both isoGSM and sampling measurement showed high precipitation $\delta^{18}O$ in May, and reached relatively low values in the wet season during August and September. However, the original isoGSM data tended to overestimate the measured precipitation $\delta^{18}O$ in the sampling periods (Fig. 2a). From downstream to upstream, the amount weighted average precipitation $\delta^{18}O$ of samples collected at the four stations (Nuxia, Yangcun, Nugesha and Lazi) were -9.58‰, -14.01‰, -14.80‰ and -17.86‰, respectively, while the corresponding weighted average values of isoGSM pixels containing the sampling stations during the same period were -7.53‰, -8.38‰, -9.22‰ and -9.61%, respectively. Bias between isoGSM data and sampling measurement tended to be larger at upstream stations with higher elevations, partly due to the coarse spatial resolution of GCM which cannot reproduce the effect of regional topography well. In contrast, the corrected isoGSM data (black lines in Fig. 3a) captured the relatively low values in the late wet season better than the original data (grey lines in Fig. 3a), and the scatter points fall closer to the 1:1 line (Fig. 2b). The MAE of isoGSM precipitation $\delta^{18}O$ in the YTR reduced from 6.65‰ to 4.91‰ after correction. Similarly, the original isoGSM data presented comparable seasonal

https://doi.org/10.5194/hess-2021-244
Preprint. Discussion started: 28 May 2021


Hydrology and Earth System Sciences
Discussions
Open Access
EGU

fluctuations of precipitation isotope to the sampling measurement at the Wengguo station in the KR catchment (Fig. 3b), but the amount weighted average of precipitation $\delta^{18}O$ in the original isoGSM data (-10.95‰) is much higher than that in the sampling measurement (-15.97‰, Fig. 2c and 3b). After bias correction, the overestimation was much reduced (Fig. 2d), indicated by a reduced MAE value from 6.24‰ to 4.47‰. Underestimation of precipitation $\delta^{18}O$ by the original isoGSM data in springs of 2011 and 2012, however, was not improved by the bias correction.

[Figure 2]

[Figure 3]

Based on the multiple linear regression, the coefficients *x*, *y* and *z* in Eq. 1 were estimated as -0.003, 0.574 and -52.6, respectively, to interpolate the measured isotope data to estimate spatial precipitation isotope over the YTR basin. Parameters *a* and *b* in Eq. 3 were estimated as -0.0046 and 14.96 based on the biases between isoGSM data and sampling measurements on the four sampling sites in YTR. Fig. 4 shows the comparison of the amount weighted averages of precipitation $\delta^{18}O$ on 63 REWs derived from the corrected isoGSM data and interpolated sampling measurement. It is shown that the distributions of precipitation isotope with altitude were rather similar in the two datasets (Fig. 4b). However, distributions across the longitudes show visible differences (Fig. 4a). In comparison to the corrected isoGSM data, the interpolated sampling measurement estimated much lower isotope signature in the west upstream region (longitude <86°), while presenting higher the isotope signature in the east middle and downstream regions (longitude falls between 91° and 93°). As site sampling data of precipitation was insufficient to test which of the two datasets captured the west-east distribution of precipitation isotope better, model performance on simulating isotope signatures of stream water measured at hydrological stations from west to east forced by the two datasets provide a perspective to assess the precipitation isotope estimations.

[Figure 4]

3.2 Model performance for the simulations of discharge and stream water isotope

Fig. 5-6 and Table 3 show the model performance of different calibration variants in the YTR basin produced by the behavioral parameter sets. The three calibration variants produced similar simulations of discharge and SCA (Fig. 5), in spite of the slightly higher NSE_{dis} and lower $RMSE_{SCA}$ estimated by the dual-objective calibration (Table 3). For the simulation of stream water $\delta^{18}O$, the dual-objective calibration produced the worst MAE_{iso} values in three out of the four testing stations with the largest uncertainty ranges (Fig. 6a), which can be expected as isotope data was not involved in this calibration. The two triple-objective calibration variants produced good simulation for the stream water isotope at the Nuxia station in the calibration year of 2005 (Fig. 6b and 6c). However, the triple-objective calibration variant forced by

https://doi.org/10.5194/hess-2021-244
Preprint. Discussion started: 28 May 2021

isoGSM data estimated worse performance (i.e., higher MAE_{iso} values) for stream water $\delta^{18}O$ at the stations of Yangcun and Nugesha than the calibration forced by interpolated sampling measurement showing significant underestimations for peak isotope values in June at Yangcun station, and higher overestimations for isotope values after August at Nugesha. This was due to the poor performance of isoGSM on capturing the isotope signature of individual precipitation events during a specific period (see Fig. 3a), although being corrected already. For example, the amount weighted average of measured precipitation $\delta^{18}O$ in June at the Yangcun station was -5.87‰, while the average of corrected isoGSM data showed a value of -10.09‰, leading to an underestimated peak value. Similarly, the amount weighted average of measured precipitation $\delta^{18}O$ at Nugesha during August was -16.34‰, while the corrected isoGSM data estimated an average of -11.47‰, leading to an overestimated stream $\delta^{18}O$ in the late wet season. In spite of that, the performance of simulated stream water $\delta^{18}O$ at Nuxia, Yangcun and Nugesha stations forced by corrected isoGSM data can still be considered as acceptable, given the MAE_{iso} values were generally around 1 (Fig. 6c). For the most upstream station Lazi, however, the triple-objective variant forced by measured precipitation $\delta^{18}O$ produced significantly underestimated $\delta^{18}O$ of stream water, likely due to the underestimated precipitation $\delta^{18}O$ in the upstream high altitudes produced by the interpolated measurement data (Fig. 4b). The good performance of simulated stream water $\delta^{18}O$ at the Lazi station driven by the corrected isoGSM data demonstrated that the corrected isoGSM estimated a better precipitation isoscape in high altitudes of the study catchment than the linearly interpolated measurement data, partly benefiting from the information of spatial precipitation isotope implied in the gridded values. It is worth noting that the model simulations forced by corrected isoGSM estimated narrower uncertainty bands for stream water $\delta^{18}O$ at Nuxia, Yangcun and Nugesha, and smaller value ranges of the MAE_{iso} metric at all the four stations, in comparison to the simulations driven by the interpolated precipitation $\delta^{18}O$. Compared to the simulations yielded by the dual-objective calibration, the triple-objective calibration variants simulated smaller uncertainty ranges for stream water $\delta^{18}O$ and slightly narrowed value ranges of objective metrics for the simulations of discharge and SCA with the lower behavioral ratios of calibrated parameter sets in Table 3, indicating good potential of isotope data on reducing modeling uncertainty and improving parameter identifiability.

[Figure 5]

[Figure 6]

[Table 3]

The simulated hydrographs at two internal hydrological stations of Yangcun and Nugesha were compared in Fig. 7 to assess the spatial consistency of model parameters calibrated by the different variants. The isoGSM-forced triple-objective calibration produced the highest performance for discharge simulation at the two internal stations (Fig. 7e and 7f) indicated by

https://doi.org/10.5194/hess-2021-244
Preprint. Discussion started: 28 May 2021

the highest averages (0.82 and 0.74 for Yangcun and Nugesha) and minimal values (0.72 and 0.53 for Yangcun and Nugesha) of NSE, as well as the smallest values ranges of NSE. The dual-objective calibration produced lower performance for discharge simulation than the isoGSM-forced triple-objective calibration (with average NSE as 0.8 and 0.67 at Yangcun and Nugesha) with a much larger uncertainty of the baseflow simulation (Fig. 7a and Fig. 7b). The measurement-forced triple-objective calibration produced higher mean NSE (0.81 and 0.74 for Yangcun and Nugesha) but smaller minimal NSE (0.62 and 0.31 for Yangcun and Nugesha) than the dual-objective calibration with the largest values ranges of NSE at the two stations. Moreover, the isoGSM-forced triple-objective calibration performed best on capturing the peak flows in summer at both stations.

[Figure 7]

The model performances produced by the behavioral parameter sets of different calibration variants in the KR catchment were shown in Figs. 8-9 and Table 4. All the three calibration variants presented similar performances on simulating streamflow, while the two triple-objective calibrations resulted in narrower uncertainty ranges, especially for the baseflow (Fig. 8c and e). The declining SCA in spring-summer was captured well in all the calibration variants (Figs. 8b, d and f). Triple-objective calibrations driven by the two isotope datasets performed comparably well on simulating the isotopic composition of stream water in the calibration period (Fig. 9b and 9c) indicated by the low average values of MAE_{iso} (0.68 and 0.69) and the well captured seasonal fluctuations of stream water $\delta^{18}O$. The peak isotopic values in around June of 2007 were not captured well by the isoGSM-driven model (Fig. 9c), resulting in a relatively larger minimal MAE_{iso} (0.57) than the interpolated measurement-driven result (0.48). This was due to the underestimations of isoGSM on estimating the isotope signatures of individual extreme precipitation events in June (see Fig. 3b). Specifically, there was a precipitation event larger than 20mm/day in June of 2007, of which the corrected isoGSM produced significantly lower $\delta^{18}O$ (-21.55‰) than the sampling measurement (-9.83‰) at the Wengguo station. Despite that, the isoGSM-forced triple-objective calibration estimated much better performance than the interpolated measurement-driven calibration for stream water $\delta^{18}O$ in the validation period (Figs. 9b and c). Similar to YTR, the triple-objective calibrations got much smaller behavioral parameter sets (19 and 18 for measurement- and isoGSM-forced calibration variants) than the dual-objective calibration (117) through 150 runs of the automatic calibration program, indicating strongly increased identifiability of model parameters and reduced uncertainty by the using of isotope data.

[Figure 8]

[Figure 9]

[Table 4]

https://doi.org/10.5194/hess-2021-244
Preprint. Discussion started: 28 May 2021


Hydrology and Earth System Sciences
Discussions

3.3 Contributions of runoff components

Fig. 10 and Tables 5-6 compare the proportions of water sources in the annual water input for runoff generation simulated by the behavioral parameter sets identified by the three calibration variants. In the KR sub-basin (Fig. 10b and Table 6), rainfall provided the largest volume of water source for runoff generation simulated by the three calibration variants (44.2%-47.4%), followed by glacier meltwater (29.2%-33.8%). Snowmelt contributed the lowest proportion of 22.0%-23.4% in the total water input. The two triple-objective calibrations estimated very similar contributions of runoff component, and consistently estimated lower proportions of glacier melt than the dual-objective calibration, which can be attributed to the role of isotope data in regulating the contribution of strong-evaporated surface runoff component fed by glacier melt to streamflow (Nan et al., 2021) by rejecting parameter sets that estimated small proportions of rainfall but large proportions of glacier melt (as shown by the error bar in Fig. 10b). Meanwhile, uncertainties of the estimated contributions were significantly reduced (from 9.4% to 6.2% and 4.7%, Table 6) by integrating isotope data into the model. Regarding the contributions of water sources to seasonal water input, snowmelt and rainfall were the dominant water sources in spring and summer. Three water sources had similar contributions during autumn. Glacier melt produced a relatively steady contribution of around 30%-35% throughout the year. Similar to the annual contributions, seasonal contributions of snowmelt and rainfall estimated by the two triple-objective calibrations were larger than those estimated by the dual-objective calibration, while the opposite holds true for the seasonal contributions of glacier melt. The largest differences of the contributions estimated by the different calibration variants go to the winter season (Table 6), which however had negligible effect on the annual runoff regime because of the extremely low contribution of water input in this season (<1%). Uncertainties of the runoff component contributions were reduced by involving isotope calibration most significantly during summer, because the isotope data brought more constraint on the rainfall-runoff processes, which played dominant role in summer. The uncertainties of annual contributions were close to those of summer contributions because of the large proportion of water input to annual runoff in summer (>60%). In contrast, uncertainties of winter contributions estimated by the triple-objective calibration variants tended to be larger than that estimated by the dual-objective calibration, due to the smaller amount of total water input in winter as a result of lower contribution of meltwater estimated by triple-objective variants.

In the YTR catchment, rainfall showed larger dominance on annual runoff than glacier and snow meltwater with the mean contributions of 61.4%-69.6% (Fig. 10a and Table 5). The dual-objective calibration and triple-objective calibration forced by measured isotope data estimated similar annual contributions of rainfall (~62%), snowmelt (~11%) and glacier melt (~27%). Nonetheless, the isoGSM-forced triple-objective calibration estimated significantly higher

https://doi.org/10.5194/hess-2021-244
Preprint. Discussion started: 28 May 2021


Hydrology and Earth System Sciences
Discussions
Open Access
EGU

mean proportion of rainfall (70%) but lower mean proportion of glacier melt (18%) by rejecting the parameter sets that estimated rainfall contributions less than 60% and glacier melt contributions more than 30%, which however were identified to be acceptable in the other two calibration variants (as shown by the error bar in Fig. 10a). Difference of the glacier melt contributions estimated by the two triple-objective calibration variants mainly resulted from the difference of precipitation $\delta^{18}O$ inputs from the two datasets. The interpolated measurement data tended to produce higher precipitation $\delta^{18}O$ in the middle and downstream regions of YTR basin but lower values in the upstream region, compared to the corrected isoGSM data (Fig. 4b). Meanwhile, the precipitation input in the downstream region was higher than that occurred in the upstream (Xu et al., 2017), thus resulting in higher average precipitation $\delta^{18}O$ over the entire YTR of the interpolated measurement data. Consequently, larger contribution of glacier melt with low isotope composition was estimated in the interpolated measurement-forced triple-objective calibration to counteract the effect of precipitation input with high isotopic composition for matching the measured stream water $\delta^{18}O$. By involving isotope simulation, both triple-objective variants significantly reduced the uncertainties of the estimated contributions (from 11.9% to 8.6% and 8.9%, Table 5). Similar to the estimated annual contributions, the isoGSM-forced triple-objective calibration estimated higher mean proportion of rainfall, lower mean proportion of glacier melt and comparable mean proportion of snowmelt in the four seasons, compared to the dual-objective calibration and triple-objective calibration forced by measured isotope data. In general, rainfall was the dominant water input source in summer and autumn, and snowmelt dominated the runoff in winter. The contributions of rainfall and snowmelt to total water input were close in spring. Similar to KR catchment, uncertainty of runoff component contribution was reduced by the isotope-involved calibrations more significantly in seasons when rainfall played dominant roles.

[Figure 10]

[Table 5]

[Table 6]

4. Discussion

4.1 Uncertainties of the simulations of water isotope signatures

Integrating the simulations of water isotope signatures into the hydrological model structure could help to make use of hydrological information additionally implied in the water isotope data without introducing new model parameters for the runoff processes. However, uncertainty of the simulation of water isotope in the tracer-aided hydrological model can be caused by the following sources. First, the isotopic compositions of meltwater sources were determined based on simplified assumptions, which however were hard to verify in a large

https://doi.org/10.5194/hess-2021-244
Preprint. Discussion started: 28 May 2021


Hydrology and Earth System Sciences
Discussions
Open Access
EGU

basin due to the limited field sampling work. The isotopic compositions of glacier melt were assumed as constant throughout the modeling period due to the unavailability of glacier melting water samples. This could be reasonable because the changes of glacier elevation during the 10-year modeling period were small, indicating that ice melt on the glacier surface in each of the summer seasons occurred very likely from the same elevation bands with similar isotopic compositions. The isotopic evolution of snow meltwater was simulated according to the mass balance of snowpack. The isotope fractionation effect caused by the melt processes was inadequately characterized in our model, which could lead to uncertainty in the simulation of snowmelt isotope (Pu et al., 2020).

Second, the uncertainty of the precipitation isotope input data served as another uncertainty source of the isotope simulation in the model. Although the isotope data itself had no influences on the hydrological processes, the calibration procedure to fit the simulated stream isotope signature with observation indeed affected the model simulations of runoff processes (Delavau et al., 2017). For the sampling measurement-based forcing data, the uncertainty came from the interpolation procedure. We used a linear interpolation method based on longitude and altitude to estimate the precipitation isoscape. This could be reasonable in our study catchment because these two factors characterize the major spatial pattern and altitude effect of precipitation isotope in similar large-scale regions on TP (Liu et al., 2014). However, low availability of site measurement data derived from the sparse water sampling network leaded to large uncertainty of the interpolated result. Measurements from more water sampling sites are required in the future for the improvement of the interpolation method. For the isoGSM data, uncertainty came from its coarse spatial resolution. Although the isoGSM data bears the potential to capture spatial patterns of precipitation isotope in large basins, the effect of regional topography on isotope was not reflected well in the current product due to its rather coarse pixel size (~200km×200km). Consequently, developing downscale methods that are applicable to mountainous catchments to extract regional isotope estimates from iGCM products (such as iRCM in Sturm et al., 2007) might be helpful for the tracer-aided hydrological modelling on the TP. Moreover, the bias-correction procedure based on measurements from a sparse water sampling network inevitably brought uncertainty to the corrected isoGSM data. The current sampling sites of precipitation are located along the river channel with elevations lower than the contributing mountains, thus failing to involve isoGSM estimates at high mountainous terrains into the correction procedure.

4.2 The value of spatial precipitation isotope data derived from iGCM for aiding hydrological modeling in large basins

Comparisons with the dual-objective calibration without isotope data indicated high value of spatial precipitation isotope data for reducing modeling uncertainty. Model simulations

https://doi.org/10.5194/hess-2021-244
Preprint. Discussion started: 28 May 2021

forced by the two precipitation isotope datasets produced similar total streamflow simulation in the YTR basin, but resulted in certain difference in the simulated stream water isotopic composition and water source apportionments, which was consistent with the findings in Delavau et al. (2017). The choice of precipitation isotope input data was demonstrated to have large influence on the model performance. In this study, model simulations forced by the corrected isoGSM data performed better than that driven by the interpolated data of sampling measurement with respect to discharge and stream water isotope simulations at internal hydrological stations. Beyond that, the runoff component contributions estimated by the isoGSM-forced triple-objective calibration were likely more reliable than those estimated by the dual-objective and the measurement-forced triple-objective calibrations. Contribution of glacier melt to annual water input in the YTR basin was estimated as around 27% in the dual-objective and the measurement-forced triple-objective calibrations, which might not be reasonable, considering the small glacier covered area ratio (2%). Glacier melt contribution estimated by the isoGSM-forced triple-objective calibration was lower than 20%, similarly to estimates in some previous studies (Immerzeel et al., 2010; Bookhagen and Burbank, 2010; Zhang et al., 2013), and the finding that glacier melt contributed a bit more than snowmelt was consistent with the result of Lutz et al. (2014) during the similar period (1998-2007).

This indicated that the corrected isoGSM product served as a better choice to force the tracer-aided hydrological model than the interpolated data of sampling measurement. It is commonly difficult to estimate the precipitation isoscapes in large mountainous catchments according to limited available site sampling data. Relatively, the iGCM data has the advantage of presenting more spatial information of precipitation isotope via physically simulating the processes of vapor transfer, condensation and supersaturation in the atmosphere and their effects on precipitation isotope (Xi, 2014). Our results indicated that even precipitation isotope measurements at only four sampling sites provided sounds good ground data basis to correct the isoGSM isotope product in the study basin with a size of 2×10^5 km^2. The condition was different in the KR sub-catchment, where the triple-objective variants forced by two isotope datasets performed similarly with respect to discharge and isotope simulation and runoff component contribution estimation. This is due to the much smaller catchment area than the pixel size, thus the advantage of the spatial information provided by isoGSM was not taken adequately.

5. Conclusions

The utility of precipitation isotope input derived from the Isotopic General Circulation Models (iGCM) product isoGSM in forcing the distributed tracer-aided hydrological model THREW-t in a large basin of 2×10^5km^2 on the Tibetan Plateau (TP) was investigated in this work. Model performance driven by the isoGSM data was evaluated by comparing with

https://doi.org/10.5194/hess-2021-244
Preprint. Discussion started: 28 May 2021

simulations driven by precipitation isotope measurements from a sparse sampling network. Our main findings are:

(1) Spatial precipitation isotope data derived from the Isotopic General Circulation Models helped to reduce modeling uncertainty and improve parameter identifiability, in comparison to a calibration method using discharge and snow cover area fraction without any information of water isotope. The developed tracer-aided hydrological model forced by the isoGSM data showed high values for robustly representing runoff processes in large mountainous catchments.

(2) Model parameters estimated by the isoGSM data corrected using site sampling measurements of precipitation isotope presented higher transferability to nested sub-basins and produced higher model performance in the validation period than that estimated by the interpolated isotope data from site sampling measurement. The smaller uncertainty ranges of model simulations in nested sub-basins forced by the corrected isoGSM data further indicated that the corrected isoGSM data served as a better choice to provide informative spatial precipitation isotope in large basins than the interpolated data from site sampling measurements.

(3) Using the corrected isoGSM data improved the quantification of contributions of runoff components to streamflow on both annual and seasonal scales. Model calibration procedure forced by the corrected isoGSM data successfully rejected parameter sets that estimated overestimation of glacier melt contribution, indicating that precipitation isotope measurements at only four sampling sites along the river channel provided a good ground data basis to correct the isoGSM product in the study catchment.

Code/Data availability

The isotope data and the code of THREW-t model used in this study are available by contacting the authors.

Author contribution

YN, ZH and FT conceived the idea; ZW provided the isoGSM data; LT provided the measurement isotope data; YN, ZH and FT conducted analysis; ZW and LT provided comments on the analysis; all the authors contributed to writing and revisions.

Competing interests

The authors declare that they have no conflict of interest.

Acknowledgements

This study was supported by the National Science Foundation of China (92047301, 51825902, 91647205). The authors thank all the organizations and scientists for the contribution of data

https://doi.org/10.5194/hess-2021-244
Preprint. Discussion started: 28 May 2021


Hydrology and Earth System Sciences
Discussions
Open Access
EGU

578 used in this work. All the data used in this study will be available on request from the
579 corresponding author (tianfq@mail.tsinghua.edu.cn).

580 **Financial support**

581 This study was supported by the National Science Foundation of China (grant no. 92047301,
582 51825902, 91647205).
583

https://doi.org/10.5194/hess-2021-244
Preprint. Discussion started: 28 May 2021

584 **References**

585 Ala-aho, P., Tetzlaff, D., McNamara, J. P., Laudon, H., & Soulsby, C. (2017). Using isotopes to
586 constrain water flux and age estimates in snow-influenced catchments using the STARR
587 (Spatially distributed Tracer-Aided Rainfall–Runoff) model. Hydrology and Earth System
588 Sciences, 21(10), 5089-5110. doi:10.5194/hess-21-5089-2017

589 Birkel, C., & Soulsby, C. (2015). Advancing tracer-aided rainfall-runoff modelling: a review of
590 progress, problems and unrealised potential. Hydrological Processes, 29(25), 5227-5240.
591 doi:10.1002/hyp.10594

592 Birkel, C., Tetzlaff, D., Dunn, S. M., & Soulsby, C. (2011). Using time domain and geographic
593 source tracers to conceptualize streamflow generation processes in lumped rainfall-runoff
594 models. Water Resources Research, 47(2). doi:10.1029/2010wr009547

595 Bookhagen, B., & Burbank, D. W. (2010). Toward a complete Himalayan hydrological budget:
596 Spatiotemporal distribution of snowmelt and rainfall and their impact on river discharge.
597 Journal of Geophysical Research, 115(F3). doi:10.1029/2009jf001426

598 Capell, R., Tetzlaff, D., & Soulsby, C. (2012). Can time domain and source area tracers reduce
599 uncertainty in rainfall-runoff models in larger heterogeneous catchments? Water
600 Resources Research, 48(9). doi:10.1029/2011wr011543

601 Chen, X., Long, D., Liang, S., He, L., Zeng, C., Hao, X., & Hong, Y. (2018). Developing a
602 composite daily snow cover extent record over the Tibetan Plateau from 1981 to 2016
603 using multisource data. Remote Sensing of Environment, 215, 284-299.
604 doi:10.1016/j.rse.2018.06.021

605 Delavau, C. J., Stadnyk, T., & Holmes, T. (2017). Examining the impacts of precipitation
606 isotope input (δ18O) on distributed, tracer-aided hydrological modelling. Hydrology and
607 Earth System Sciences, 21(5), 2595-2614. doi:10.5194/hess-21-2595-2017

608 Didan, K. (2015). MOD13A3 MODIS/Terra vegetation Indices Monthly L3 Global 1km SIN
609 Grid V006 [Data set]. NASA EOSDIS Land Processes DAAC. Accessed 2020-01-01 from
610 https://doi.org/10.5067/MODIS/MOD13A3.006

611 Dong, W., Lin, Y., Wright, J. S., Ming, Y., Xie, Y., Wang, B., . . . Xu, F. (2016). Summer rainfall
612 over the southwestern Tibetan Plateau controlled by deep convection over the Indian
613 subcontinent. Nature Communications, 7. doi:10.1038/ncomms10925

https://doi.org/10.5194/hess-2021-244
Preprint. Discussion started: 28 May 2021

614 Duethmann, D., Bolch, T., Farinotti, D., Kriegel, D., Vorogushyn, S., Merz, B., . . . Güntner, A.
615 (2015). Attribution of streamflow trends in snow and glacier melt-dominated catchments
616 of the Tarim River, Central Asia. Water Resources Research, 51(6), 4727-4750.
617 doi:10.1002/2014wr016716

618 Eriksson, D., Bindel, D., & Shoemaker, C. (2015). Surrogate optimization toolbox (pysot).

619 Gao, J., Tian, L. D., & Liu, Y. Q. (2009). Oxygen isotope variation in the water cycle of the
620 Yamdrok-tso Lake Basin in southern betan Plateau. Chinese Science Bulletin, 54(15),
621 2153-2159.

622 Gupta, H. V., Wagener, T., & Liu, Y. (2008). Reconciling theory with observations: elements of
623 a diagnostic approach to model evaluation. Hydrological Processes, 22(18), 3802-3813.
624 doi:10.1002/hyp.6989

625 He, Z., Unger-Shayesteh, K., Vorogushyn, S., Weise, S. M., Kalashnikova, O., Gafurov, A., . . .
626 Merz, B. (2019). Constraining hydrological model parameters using water isotopic
627 compositions in a glacierized basin, Central Asia. Journal of Hydrology, 571, 332-348.
628 doi:10.1016/j.jhydrol.2019.01.048

629 He, Z., Vorogushyn, S., Unger-Shayesteh, K., Gafurov, A., Kalashnikova, O., Omorova, E., &
630 Merz, B. (2018). The Value of Hydrograph Partitioning Curves for Calibrating
631 Hydrological Models in Glacierized Basins. Water Resources Research, 54(3), 2336-2361.
632 doi:10.1002/2017wr021966

633 He, Z. H., Tian, F. Q., Gupta, H. V., Hu, H. C., & Hu, H. P. (2015). Diagnostic calibration of a
634 hydrological model in a mountain area by hydrograph partitioning. Hydrology and Earth
635 System Sciences, 19(4), 1807-1826. doi:10.5194/hess-19-1807-2015

636 He, Z., Yang, L., Tian, F., Ni, G., Hou, A., & Lu, H. (2017). Intercomparisons of Rainfall
637 Estimates from TRMM and GPM Multisatellite Products over the Upper Mekong River
638 Basin. Journal of Hydrometeorology, 18(2), 413-430. doi:10.1175/jhm-d-16-0198.1

639 Hindshaw, R. S., Tipper, E. T., Reynolds, B. C., Lemarchand, E., Wiederhold, J. G., Magnusson,
640 J., . . . Bourdon, B. (2011). Hydrological control of stream water chemistry in a glacial
641 catchment (Damma Glacier, Switzerland). Chemical Geology, 285(1-4), 215-230.
642 doi:10.1016/j.chemgeo.2011.04.012

643 Immerzeel, W. W., Pellicciotti, F., & Bierkens, M. F. P. (2013). Rising river flows throughout
644 the twenty-first century in two Himalayan glacierized watersheds. Nature Geoscience, 6(9),

742-745. doi:10.1038/ngeo1896

Immerzeel, W. W., van Beek, L. P. H., & Bierkens, M. F. P. (2010). Climate Change Will Affect the Asian Water Towers. Science, 328(5984), 1382-1385. doi:10.1126/science.1183188

Kanamitsu, M., Kumar, A., Juang, H. M. H., Schemm, J. K., Wang, W. Q., Yang, F. L., . . . Ji, M. (2002). NCEP dynamical seasonal forecast system 2000. Bulletin of the American Meteorological Society, 83(7), 1019-+. doi:10.1175/1520-0477(2002)083<1019:Ndsfs>2.3.Co;2

Liu, J., Song, X., Yuan, G., Sun, X., & Yang, L. (2014). Stable isotopic compositions of precipitation in China. Tellus Series B-Chemical and Physical Meteorology, 66. doi:10.3402/tellusb.v66.22567

Liu S. (2012). The second glacier inventory dataset of China (version 1.0) (2006-2011) [Data set]. National Tibetan Plateau Data Center. Accessed 2020-01-01 from https://doi.org/10.3972/glacier.001.2013.db.

Liu, Z., Tian, L., Yao, T., Gong, T., Yin, C., & Yu, W. (2007). Temporal and spatial variations of delta O-18 in precipitation of the Yarlung Zangbo River Basin. Journal of Geographical Sciences, 17(3), 317-326. doi:10.1007/s11442-007-0317-1

Lutz, A. F., Immerzeel, W. W., Shrestha, A. B., & Bierkens, M. F. P. (2014). Consistent increase in High Asia's runoff due to increasing glacier melt and precipitation. Nature Climate Change, 4(7), 587-592. doi:10.1038/nclimate2237

Masood, M., Yeh, P. J. F., Hanasaki, N., & Takeuchi, K. (2015). Model study of the impacts of future climate change on the hydrology of Ganges–Brahmaputra–Meghna basin. Hydrology and Earth System Sciences, 19(2), 747-770. doi:10.5194/hess-19-747-2015

Myneni, R., Knyazikhin, Y., Park, T. (2015). MOD15A2H MODIS/Terra Leaf Area Index/FPAR 8-Day L4 Global 500m SIN Grid V006 [Data set]. NASA EOSDIS Land Processes DAAC. Accessed 2020-01-01 from https://doi.org/10.5067/MODIS/MOD15A2H.006

Nan, Y., Tian, L., He, Z., Tian, F., & Shao, L. (2021). The value of water isotope data on improving process understanding in a glacierized catchment on the Tibetan Plateau. Hydrology and Earth System Sciences Discussions. doi:10.5194/hess-2021-134

Noone, D., & Sturm, C. (2010). Comprehensive Dynamical Models of Global and Regional

https://doi.org/10.5194/hess-2021-244
Preprint. Discussion started: 28 May 2021

675 Water Isotope Distributions.

676 Pu, T., Wang, K., Kong, Y., Shi, X., Kang, S., Huang, Y., . . . Cuntz, M. (2020). Observing and
677 Modeling the Isotopic Evolution of Snow Meltwater on the Southeastern Tibetan Plateau.
678 Water Resources Research, 56(9). doi:10.1029/2019wr026423

679 Schaner, N., Voisin, N., Nijssen, B., & Lettenmaier, D. P. (2012). The contribution of glacier
680 melt to streamflow. Environmental Research Letters, 7(3). doi:10.1088/1748-
681 9326/7/3/034029

682 Son, K., & Sivapalan, M. (2007). Improving model structure and reducing parameter
683 uncertainty in conceptual water balance models through the use of auxiliary data. Water
684 Resources Research, 43(1). doi:10.1029/2006wr005032

685 Stadnyk, T. A., Delavau, C., Kouwen, N., & Edwards, T. W. D. (2013). Towards hydrological
686 model calibration and validation: simulation of stable water isotopes using the
687 isoWATFLOOD model. Hydrological Processes, 27(25), 3791-3810.
688 doi:10.1002/hyp.9695

689 Sturm, C., Hoffmann, G., & Langmann, B. (2007). Simulation of the stable water isotopes in
690 precipitation over South America: Comparing regional to global circulation models.
691 Journal of Climate, 20(15), 3730-3750. doi:10.1175/jcli4194.1

692 Sturm, K., Hoffmann, G., Langmann, B., & Stichler, W. (2005). Simulation of delta O-18 in
693 precipitation by the regional circulation model REMOiso. Hydrological Processes, 19(17),
694 3425-3444. doi:10.1002/hyp.5979

695 Su, F., Zhang, L., Ou, T., Chen, D., Yao, T., Tong, K., & Qi, Y. (2016). Hydrological response
696 to future climate changes for the major upstream river basins in the Tibetan Plateau. Global
697 and Planetary Change, 136, 82-95. doi:10.1016/j.gloplacha.2015.10.012

698 Tian, F., Hu, H., Lei, Z., & Sivapalan, M. (2006). Extension of the Representative Elementary
699 Watershed approach for cold regions via explicit treatment of energy related processes.
700 Hydrology and Earth System Sciences, 10(5), 619-644. doi:10.5194/hess-10-619-2006

701 Tian, F., Xu, R., Nan, Y., Li, K., & He, Z. (2020). Quantification of runoff components in the
702 Yarlung Tsangpo River using a distributed hydrological model.. Advances in Water
703 Science, 31(3), 324-336.

704 Wang, X., Zhang, X., Zhang, W., Zhang, X., & Luo, Z. (2017). Comparison on Spatial

https://doi.org/10.5194/hess-2021-244
Preprint. Discussion started: 28 May 2021

705 Distribution of Hydrogen and Oxygen Stable Isotope GCM Simulation in Global
706 Precipitation. Advance in Earth Sciences, 32(9), 983-995.

707 Wolfe, B. B., Karst-Riddoch, T. L., Hall, R. I., Edwards, T. W. D., English, M. C., Palmini,
708 R., . . . Vardy, S. R. (2007). Classification of hydrological regimes of northern floodplain
709 basins (Peace -Athabasca Delta, Canada) from analysis of stable isotopes (delta O-18,
710 delta H-2) and water chemistry. Hydrological Processes, 21(2), 151-168.
711 doi:10.1002/hyp.6229

712 Xi, X. (2014). A Review of Water Isotopes in Atmospheric General Circulation Models: Recent
713 Advances and Future Prospects. International Journal of Atmospheric Sciences, 2014, 1-
714 16. doi:10.1155/2014/250920

715 Xu, R., Hu, H., Tian, F., Li, C., & Khan, M. Y. A. (2019). Projected climate change impacts on
716 future streamflow of the Yarlung Tsangpo-Brahmaputra River. Global and Planetary
717 Change, 175, 144-159. doi:10.1016/j.gloplacha.2019.01.012

718 Xu, R., Tian, F., Yang, L., Hu, H., Lu, H., & Hou, A. (2017). Ground validation of GPM IMERG
719 and TRMM 3B42V7 rainfall products over southern Tibetan Plateau based on a high-
720 density rain gauge network. Journal of Geophysical Research: Atmospheres, 122(2), 910-
721 924. doi:10.1002/2016jd025418

722 Yang, K., He, J., Tang, W., Qin, J., & Cheng, C. C. K. (2010). On downward shortwave and
723 longwave radiations over high altitude regions: Observation and modeling in the Tibetan
724 Plateau. Agricultural and Forest Meteorology, 150(1), 38-46.
725 doi:10.1016/j.agrformet.2009.08.004

726 Yao, T., Masson-Delmotte, V., Gao, J., Yu, W., Yang, X., Risi, C., . . . Hou, S. (2013). A review
727 of climatic controls on δ18O in precipitation over the Tibetan Plateau: Observations and
728 simulations. Reviews of Geophysics, 51(4), 525-548. doi:10.1002/rog.20023

729 Yoshimura, K., Kanamitsu, M., Noone, D., & Oki, T. (2008). Historical isotope simulation
730 using Reanalysis atmospheric data. Journal of Geophysical Research, 113(D19).
731 doi:10.1029/2008jd010074

732 Zhang, F., Liu, J., Gong, T., & Wang, H. (2006). Hydrological Regime of the Karuxung
733 Watershed in North Himalayas. Acta Geographica Sinica, 61(11), 1141-1148.

734 Zhang, F., Zhang, H., Hagen, S. C., Ye, M., Wang, D., Gui, D., . . . Liu, J. (2015). Snow cover
735 and runoff modelling in a high mountain catchment with scarce data: effects of

https://doi.org/10.5194/hess-2021-244
Preprint. Discussion started: 28 May 2021


Hydrology and Earth System Sciences
Discussions

736 temperature and precipitation parameters. Hydrological Processes, 29(1), 52-65.
737 doi:10.1002/hyp.10125

738 Zhang, L., Su, F., Yang, D., Hao, Z., & Tong, K. (2013). Discharge regime and simulation for
739 the upstream of major rivers over Tibetan Plateau. Journal of Geophysical Research:
740 Atmospheres, 118(15), 8500-8518. doi:10.1002/jgrd.50665

741 Zhao, L., Xiao, H., Zhou, M., Cheng, G., Wang, L., Yin, L., & Ren, J. (2012). Factors
742 controlling spatial and seasonal distributions of precipitation d18O in China. Hydrological
743 Processes, 26(1), 143-152. doi:10.1002/hyp.8118

744 Zongxing, L., Qi, F., Zongjie, L., Ruifeng, Y., Juan, G., & Yuemin, L. (2019). Climate
745 background, fact and hydrological effect of multiphase water transformation in cold
746 regions of the Western China: A review. Earth-Science Reviews, 190, 33-57.
747 doi:10.1016/j.earscirev.2018.12.004

748

https://doi.org/10.5194/hess-2021-244
Preprint. Discussion started: 28 May 2021

List of figures

https://doi.org/10.5194/hess-2021-244
Preprint. Discussion started: 28 May 2021

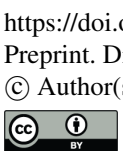

Hydrology and Earth System Sciences
Discussions
Open Access
EGU

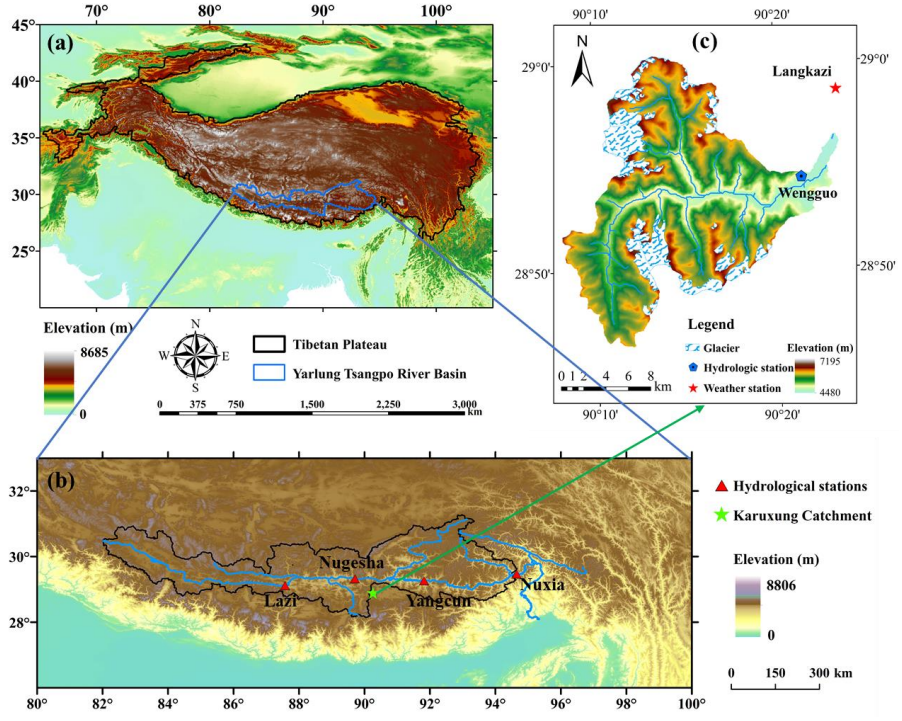

783

784 **Figure 1**. Location and topography of (a) Tibetan Plateau, (b) Yarlung Tsangpo River basin and

785 (c) Karuxung catchment

786

https://doi.org/10.5194/hess-2021-244
Preprint. Discussion started: 28 May 2021

Hydrology and Earth System Sciences
Discussions
Open Access
EGU

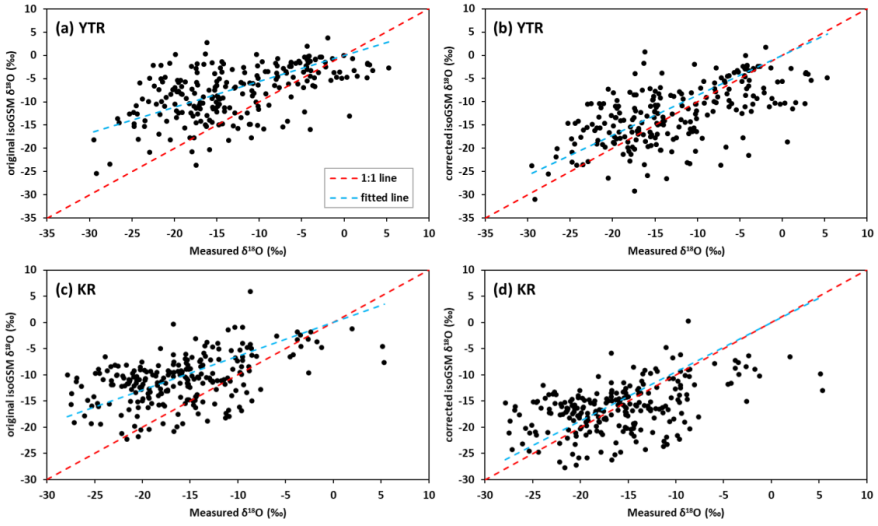

787
788 **Figure 2.** The scatter diagrams between original/corrected isoGSM and measured isotope data
789 in YTR basin (subfigures a and b) and KR catchment (subfigures c and d).
790

https://doi.org/10.5194/hess-2021-244
Preprint. Discussion started: 28 May 2021

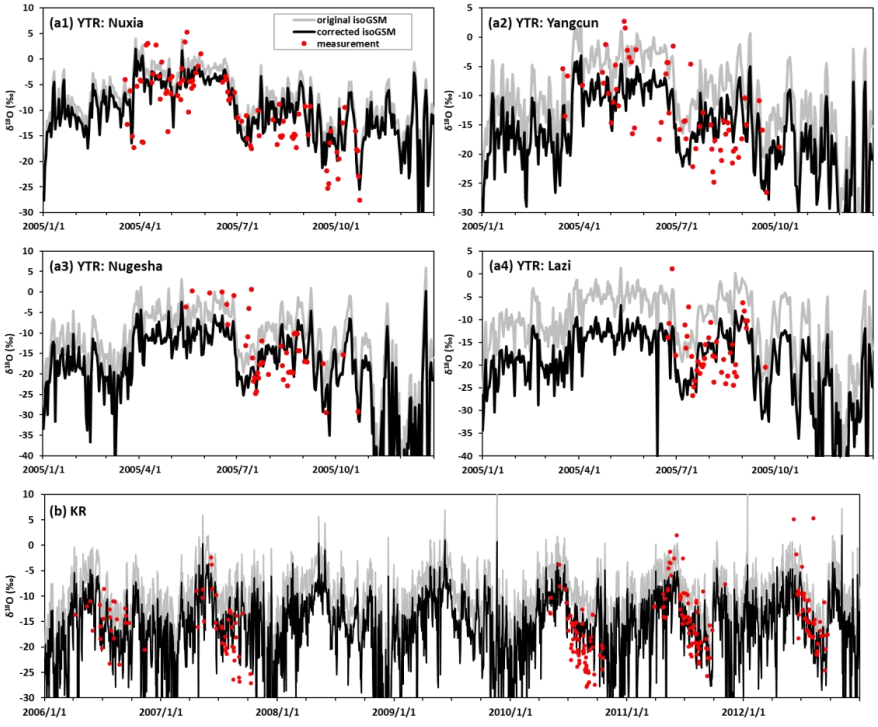

Figure 3. Temporal variations of precipitation $\delta^{18}O$ derived from measured and isoGSM data in YTR basin (subfigure a) and KR catchment (subfigure b).

https://doi.org/10.5194/hess-2021-244
Preprint. Discussion started: 28 May 2021

Hydrology and Earth System Sciences
Discussions
Open Access
EGU

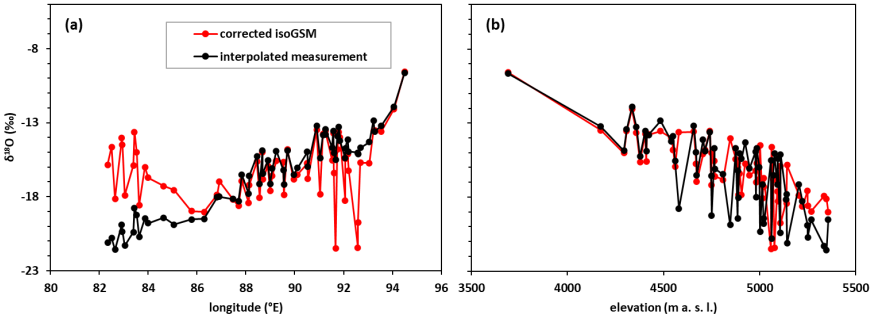

795

796 **Figure 4.** Comparisons of the amount weighted averages of precipitation $\delta^{18}O$ on 63 REWs in
797 the YTR basin by longitude (a) and elevation (b).

798

https://doi.org/10.5194/hess-2021-244
Preprint. Discussion started: 28 May 2021

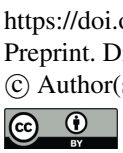

Hydrology and Earth System Sciences
Discussions
Open Access
EGU

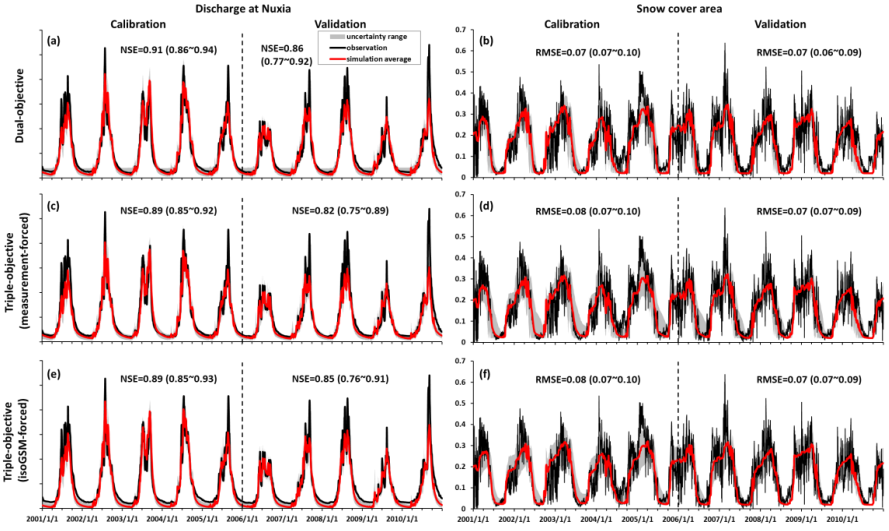

Figure 5. Uncertainty ranges of discharge and SCA simulations in YTR basin during calibration and validation periods produced by the behavioral parameter sets of the dual-objective (subfigure a and b), measurement-forced triple-objective (subfigure c and d), and isoGSM-forced triple-objective (subfigure e and f) calibration variants. The scale of discharge axis is hidden due to data security policy.

https://doi.org/10.5194/hess-2021-244
Preprint. Discussion started: 28 May 2021

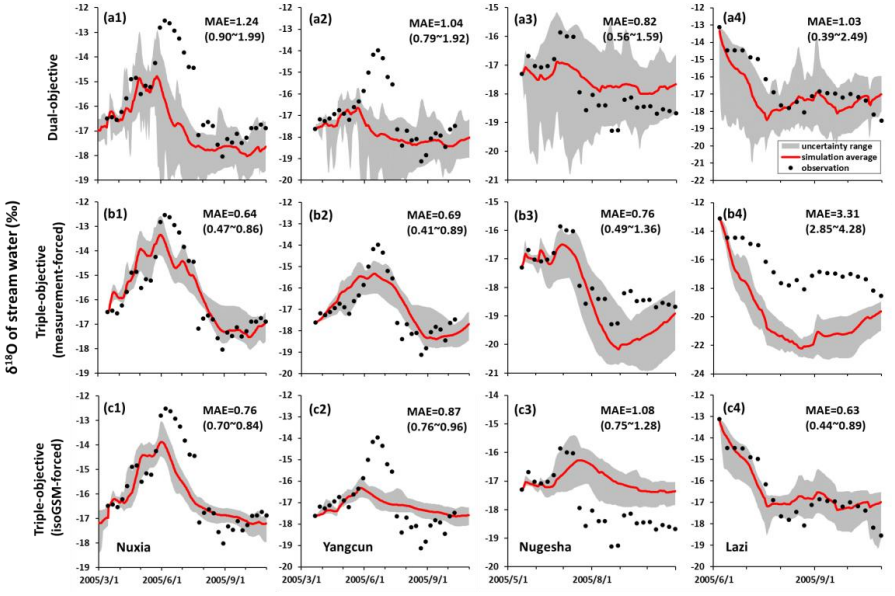

Figure 6. Uncertainty ranges of stream water $\delta^{18}O$ simulations at four stations in 2005 produced by the behavioral parameter sets of the dual-objective (a), measurement-forced triple-objective (b), and isoGSM-forced triple-objective (c) calibration variants.

https://doi.org/10.5194/hess-2021-244
Preprint. Discussion started: 28 May 2021

Hydrology and Earth System Sciences
Discussions
Open Access
EGU

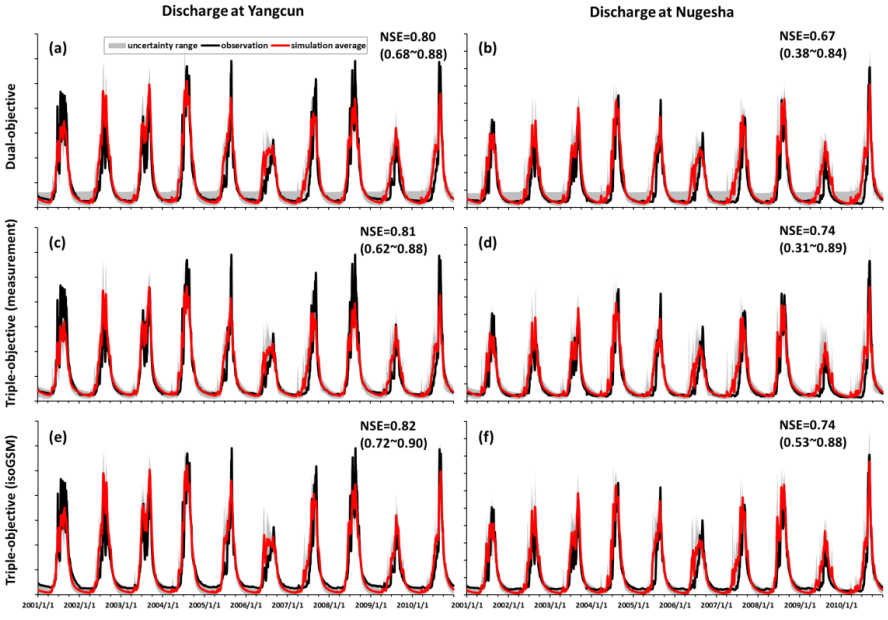

Figure 7. Uncertainty ranges of discharge simulations at Yangcun and Nugesha stations produced by the behavioral parameter sets of the dual-objective (subfigure a and b), measurement-forced triple-objective (subfigure c and d), and isoGSM-forced triple-objective (subfigure e and f) calibration variants.

https://doi.org/10.5194/hess-2021-244
Preprint. Discussion started: 28 May 2021

Hydrology and Earth System Sciences
Discussions

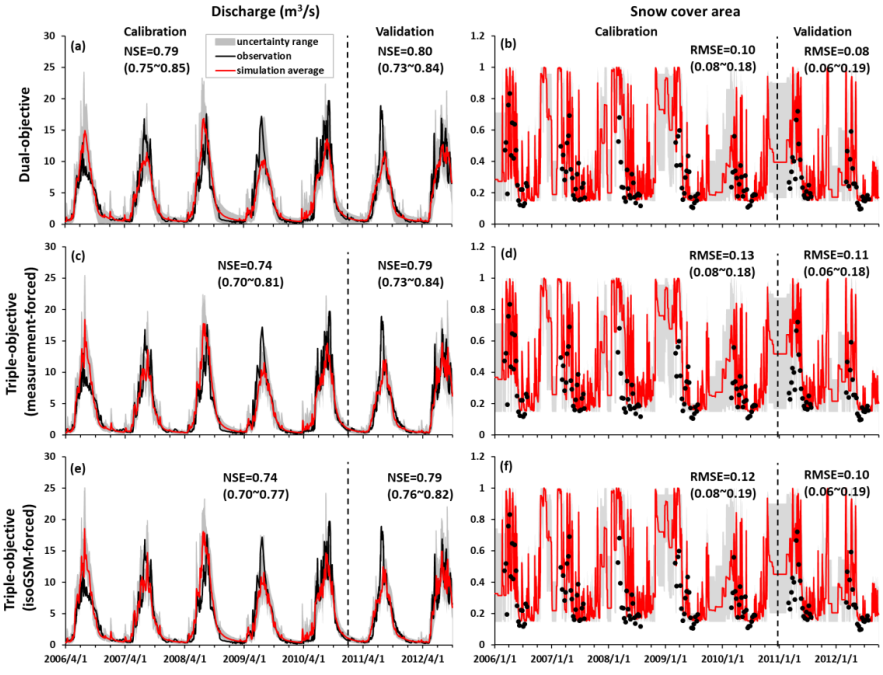

Figure 8. Uncertainty ranges of discharge and SCA simulations in KR catchment during calibration and validation periods produced by the behavioral parameter sets of the dual-objective (subfigure a and b), measurement-forced triple-objective (subfigure c and d), and isoGSM-forced triple-objective (subfigure e and f) calibration variants.

https://doi.org/10.5194/hess-2021-244
Preprint. Discussion started: 28 May 2021

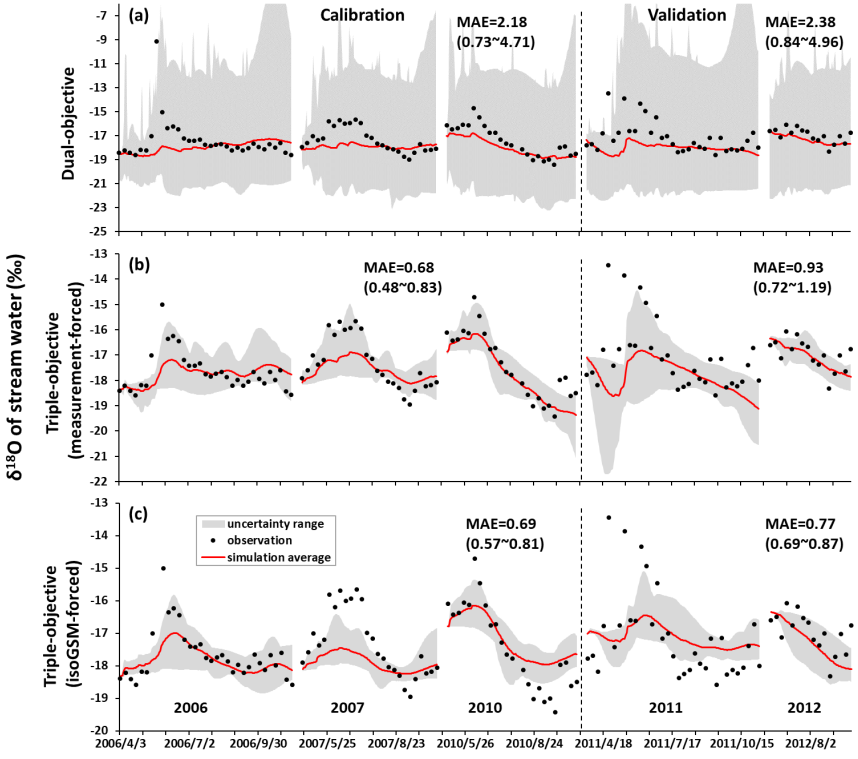

Figure 9. Uncertainty ranges of stream water $\delta^{18}O$ simulations in KR catchment during calibration and validation periods produced by the behavioral parameter sets of the dual-objective (a), measurement-forced triple-objective (b), and isoGSM-forced triple-objective (c) calibration variants.

https://doi.org/10.5194/hess-2021-244
Preprint. Discussion started: 28 May 2021

Hydrology and Earth System Sciences
Discussions
Open Access
EGU

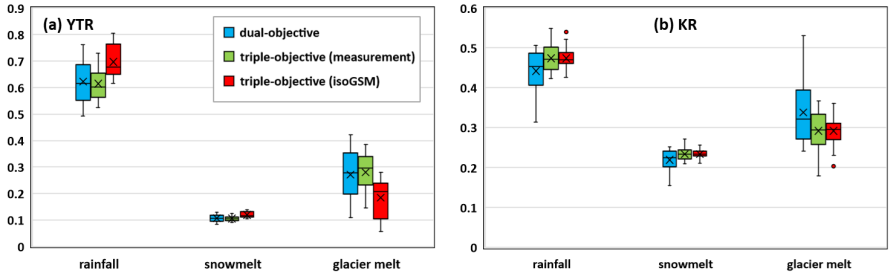

Figure 10. Average proportion and corresponding uncertainty ranges of different water sources in the annual water input for runoff generation estimated by different calibration variants in (a) YTR and (b) KR catchments.

https://doi.org/10.5194/hess-2021-244
Preprint. Discussion started: 28 May 2021


Hydrology and Earth System Sciences
Discussions

834 **List of tables**

846

https://doi.org/10.5194/hess-2021-244
Preprint. Discussion started: 28 May 2021

847 **Table 1.** Characteristics of precipitation and stream water samples in YTR and KR catchments.

Catchment (Station)	Year	Period Dd/mm to dd/mm	Precipitation sample number	Stream sample number
YTR (Nuxia)	2005	14/03 to 23/10	86	34
YTR (Yangcun)		17/03 to 05/10	59	30
YTR (Nugesha)		14/05 to 22/10	45	25
YTR (Lazi)		06/06 to 22/09	42	22
KR (Wengguo)	2006	04/06 to 11/11	24	31
	2007	23/04 to 09/10	39	25
	2010	05/05 to 18/10	63	23
	2011	28/03 to 06/11	69	32
	2012	16/06 to 22/09	42	14

848

https://doi.org/10.5194/hess-2021-244
Preprint. Discussion started: 28 May 2021

849 **Table 2.** Calibrated parameters of the THREW-t model

Symbol	Unit	Physical descriptions	Range
nt	-	Manning roughness coefficient for hillslope	0-0.2
WM	cm	Tension water storage capacity, used in Xinanjiang model (Zhao, 1992) to calculate saturation area	0-10
B	-	Shape coefficient used in Xinanjiang model to calculate saturation area	0-1
KKA	-	Coefficient to calculate subsurface runoff in $Rg=KKD \cdot S \cdot K^S_S \cdot (y_S/Z)^{KKA}$, where S is the topographic slope, K^S_S is the saturated hydraulic conductivity, y_s is the depth of saturated groundwater, Z is the total soil depth	0-6
KKD	-	See description for *KKA*	0-0.5
T_0	℃	Temperature threshold above which snow and glacier melt	-5-5
DDF_N	mm/℃/day	Degree day factor for snow	0-10
DDF_G	mm/℃/day	Degree day factor for glacier	0-10
C1	-	Coefficient to calculate the runoff concentration process using Muskingum method: $O_2=C_1 \cdot I_1+C_2 \cdot I_2+C_3 \cdot O_1+C_4 \cdot Q_{lat}$, where I_1 and O_1 is the inflow and outflow at prior step, I_2 and O_2 is the inflow and outflow at current step, Q_{lat} is lateral flow of the river channel, $C_3=1-C_1-C_2$, $C_4=C_1+C_2$	0-1
C2	-	See description for *C1*	0-1

850

https://doi.org/10.5194/hess-2021-244
Preprint. Discussion started: 28 May 2021

Hydrology and Earth System Sciences
Discussions
Open Access
EGU

851 **Table 3.** Comparisons of the model performance in YTR basin produced by different calibration
852 variants.

calibration variant	behavioral ratio [a]	period /station [b]	NSE_{dis} [c]	$RMSE_{SCA}$	MAE_{iso}
Dual-objective	0.98	calibration	0.91 (0.86-0.93)	0.07 (0.07-0.10)	1.24 (0.90-1.99)
		validation	0.86 (0.77-0.92)	0.07 (0.06-0.09)	0.96 (0.75~1.97)
Triple-objective (measurement)	0.64	calibration	0.89 (0.85-0.92)	0.08 (0.07-0.10)	0.64 (0.47-0.86)
		validation	0.82 (0.75-0.89)	0.07 (0.07-0.09)	1.46 (1.17-1.93)
Triple-objective (isoGSM)	0.82	calibration	0.89 (0.85-0.93)	0.08 (0.07-0.10)	0.76 (0.70-0.84)
		validation	0.85 (0.76-0.91)	0.07 (0.07-0.09)	0.87 (0.76-1.04)

853 a: Behavioral ratio represents the ratio of behavioral parameter set number to the run time of pySOT
854 program.
855 b: "Period" for discharge and SCA simulation, and "station" for isotope simulation.
856 c: Bracketed values represent the minimal and maximal values produced by the behavioral parameter
857 sets.
858

https://doi.org/10.5194/hess-2021-244
Preprint. Discussion started: 28 May 2021

Hydrology and Earth System Sciences
Discussions

859 **Table 4.** Comparisons of the model performance in KR catchment produced by different
860 calibration variants.

calibration variant	behavioral ratio	period	NSE_{dis}	$RMSE_{SCA}$	MAE_{iso}
Dual-objective	0.78	calibration	0.79	0.10	2.18
			(0.75-0.85)	(0.08-0.18)	(0.73-4.71)
		validation	0.80	0.08	2.38
			(0.73-0.84)	(0.06-0.19)	(0.84-4.96)
Triple-objective	0.13	calibration	0.74	0.13	0.68
(measurement)			(0.70-0.81)	(0.08-0.18)	(0.48-0.83)
		validation	0.79	0.11	0.93
			(0.73-0.84)	(0.06-0.18)	(0.72-1.19)
Triple-objective	0.12	calibration	0.74	0.12	0.69
(isoGSM)			(0.70-0.77)	(0.08-0.19)	(0.57-0.81)
		validation	0.79	0.10	0.77
			(0.76-0.82)	(0.06-0.19)	(0.69-0.87)

861

https://doi.org/10.5194/hess-2021-244
Preprint. Discussion started: 28 May 2021

Hydrology and Earth System Sciences
Discussions
Open Access
EGU

862 **Table 5.** Average proportions of water sources in the annual and seasonal water inputs for
863 runoff generation in YTR basin.

Season	Water source [a]	Dual-objective	Triple-objective (measurement)	Triple-objective (isoGSM)
Annual	Rainfall	62.2	61.4	69.6
	Snow melt	10.7	10.6	12.0
	Glacier melt	27.1	28.0	18.4
	Uncertainty	11.4	8.6	8.9
Spring	Rainfall	35.4	36.8	44.2
	Snow melt	42.9	39.7	43.8
	Glacier melt	21.7	23.5	12.0
	Uncertainty	13.4	12.8	11.8
Summer	Rainfall	69.8	68.2	74.5
	Snow melt	3.4	4.4	6.4
	Glacier melt	26.8	27.4	19.1
	Uncertainty	10.2	7.9	8.7
Autumn	Rainfall	63.1	61.9	76.1
	Snow melt	3.5	3.5	2.7
	Glacier melt	33.5	34.7	22.0
	Uncertainty	16.1	12.8	13.3
Winter	Rainfall	11.9	12.8	30.8
	Snow melt	70.1	65.8	61.7
	Glacier melt	18.0	21.4	7.5
	Uncertainty	19.7	20.6	30.8

864 a: The uncertainty of the contribution is defined as $E = \sqrt{{E_R}^2 + {E_N}^2 + {E_G}^2}$, where E_R, E_N and E_G
865 represent the standard deviations of the contributions of the water sources produced by the corresponding
866 behavioral parameter sets. Subscripts of R, N and G represent rainfall, snow meltwater and glacier
867 meltwater, respectively.
868

https://doi.org/10.5194/hess-2021-244
Preprint. Discussion started: 28 May 2021

869 **Table 6.** Average proportions of water sources in the annual and seasonal water inputs for
870 runoff generation in KR catchment.

Season	Water source	Dual-objective	Triple-objective (measurement)	Triple-objective (isoGSM)
Annual	Rainfall	44.2	47.4	47.4
	Snow melt	22.0	23.4	23.4
	Glacier melt	33.8	29.2	29.2
	Uncertainty	9.4	6.2	4.7
Spring	Rainfall	4.1	4.5	4.5
	Snow melt	56.3	61.6	60.9
	Glacier melt	39.5	33.9	34.6
	Uncertainty	13.7	14.2	12.0
Summer	Rainfall	53.5	56.6	56.9
	Snow melt	14.0	15.2	15.1
	Glacier melt	32.4	28.2	28.0
	Uncertainty	9.7	5.1	3.9
Autumn	Rainfall	30.9	35.0	34.3
	Snow melt	33.9	35.3	35.5
	Glacier melt	35.1	29.7	30.3
	Uncertainty	11.2	11.0	9.6
Winter	Rainfall	0	0	0
	Snow melt	55.3	63.3	58.9
	Glacier melt	44.7	36.7	41.1
	Uncertainty	22.3	31.5	29.2

871